JOURNAL OF THEORETICAL AND APPLIED MECHANICS
61, 1, pp. 37-47, Warsaw 2023
https://doi.org/10.15632/jtam-pl/157556

STUDY ON THE STRESS INTENSITY FACTOR OF A COMPACT SPECIMEN UNDER THE PRE-COMPRESSED LOAD CONDITION

Dongquan Wu, Zixiang Liu, Dinghe Li
Sino-European Institute of Aviation Engineering, Civil Aviation University of China, Tianjin, China
Corresponding author Dongquan Wu, e-mail: dqwu@cauc.edu.cn

Zhiqiang Zhang
Aviation Engineering Institute, Civil Aviation University of China, Tianjin, China

Jianguo Chen
The 18th Research Institute of China Electronics Technology Group Corporation, Tianjin, China

Structural components are often operated under combined stress conditions (primary and secondary stresses), but the stress levels generated by residual stress (or secondary stress) is hardly ever evaluated. Hence, stress intensity factors at the crack tips of a compact tension (CT) specimen under a pre-compressed load condition are analyzed using the finite element method. Then, the average residual stress intensity factor is calculated and analyzed. As the crack length a_0/W increases, the average residual stresses σ_{ave}/σ_0 grows under the same pre-compression load. σ_{ave}/σ_0 increases rapidly at a low range of the pre-compression load but tends to a constant in a high range of the load. The distribution of the average residual stress intensity factors K_{ave} and σ_{ave}/σ_0 of the CT specimen with same crack length under different pre-compression loads have the same tendency. Additionally, the distribution of K_{ave} and K_{FEM} under different pre-compression loads are also similar. Nevertheless, K_{ave} estimated by the average residual stress is too conservative and not accurate, and the method is complex, which depends on the analysis of simulation. Therefore, a simple method for calculating Mode I stress intensity factor K for this model is presented. A group of examples is presented to verify the accuracy of the method.

Keywords: pre-compressed load, residual stress, CT specimen, stress intensity factor, finite element method

1. Introduction

The stress intensity factor (SIF) K is used to describe stress intensity or the stress state generated by a remote load or residual stresses near the crack tip in studies related to fracture mechanics (Anderson, 2005). It is usually determined for homogeneous, linear elastic materials and materials that exhibit small-scale yielding at the crack tip. The magnitude of K depends on sample geometry, size and location of the crack, magnitude and model distribution of loads acting on the material. Since the introduction of the SIF (Tada *et al.*, 2000), there have been various investigations regarding K under the primary load condition. Three modes of the SIF under different types of loads have been discussed (Rooke and Percy, 1976), and Mode I is the most common load type encountered in engineering design. Moreover, several of examples of SIFs are investigated in detail (Rooke and Percy, 1976; Sih *et al.*, 1974; Sneddon, 1946; Isida, 1966; Sih and Macdonald, 1974; Erdogan, 1962), such as in infinite plate with uniform uniaxial stress (Rooke and Percy, 1976) and infinite plate (Sneddon, 1946), etc. The American Society for Testing and Materials (ASTM) has proposed fracture toughness testing standard for different specimen modes (ASTM, 2013). The specific calculation equations of Mode I SIF for different specimens are listed in Ref. (Bower, 2009), especially the compact tension (CT) specimen, which is a common type of specimen. However, the aforementioned studies are conducted considering the primary load, but in-service components invariably develop residual stress introduced during fabrication or service processes (Chen *et al.*, 2013) (usually by thermal gradients or non-uniform plastic deformation) which may cause fracture failure. Hence, it is significant to propose computation equations to predict the SIF under the residual stress condition. Webster *et al.* (2011) obtained K of the residual stress by estimating residual stress distributions. Zhao *et al.* (2013) used this method to analyse K of the residual stress. However, the SIF is overestimated due to the residual stress field, which results in an excessively pessimistic defect assessment. To analyze the effect of residual stress on the SIF, a simple and repeatable technique of obtaining the residual stress is the pre-compression on a specific specimen (CT specimen) (Chen *et al.*, 2013; Zhao *et al.*, 2013; Xu *et al.*, 2016; Song *et al.*, 2015a,b; Shirahatti *et al.*, 2014). A tensile residual stress field in the vicinity of the crack tip can be introduced by loading a pre-compressed specimen beyond the yield strength and then unloading it (Zhao *et al.*, 2013; O'Dowd *et al.*, 2005; Turski *et al.*, 2008). Therefore, in this study, the technique of pre-compressing the CT specimen is used to investigate the effect of residual stress on the SIF. It is significant to make an appropriate prediction and derive computation equations of the SIF resulting from the residual stress.

In this study, the finite-element (FE) method was carried out to assess the effects of local tensile residual stress on the SIF. The residual stress was generated by pre-compressing the CT specimen and then unloading it. The average residual stress intensity factor was calculated and analyzed. The law of change of the SIF varied with the pre-compression load, thickness and crack length of the pre-compressed CT specimen were concluded. An analysis with a series of original computation equations was proposed to predict the SIF of the CT specimen with pre-compressed residual stress. Finally, the suitability and accuracy of the analytical method were studied and validated by comparing them with a range of examples.

2. Finite element models and material properties

2.1. Finite element models

In this study, a three-dimensional finite element (3D FE) model of the CT specimen is employed. A tensile residual stress field in the vicinity of the crack tip can be introduced by loading the pre-compressed specimen beyond the yield strength and then unloading it. This technique was previously developed by Zhao *et al.* (2013), O'Dowd *et al.* (2005), Turski *et al.* (2008).

Figure 1 shows geometry of a specified CT specimen. Thickness, width, crack depth and notch root radius of the specimen respectively are $B = 10\,\mathrm{mm}$, $W = 20\,\mathrm{mm}$, $a_0/W = 0.5$ and $r = 0.20\,\mathrm{mm}$, respectively. Only a half of the symmetric CT geometry is modelled. And the loading process is achieved by the movement of an analytical rigid shell, which is used as the punch tool. The rigid shell is constrained in the horizontal and rotational directions but free to move in the vertical direction during the loading process. The crack is inserted at the end of the notch tip after the pre-compression. Hard contact of contact control, finite sliding of sliding formulation and surface to surface of the discretization method are used in the pre-compression process. Firstly, the residual stress filed could be simulated by using the elastic-plastic finite element model, then the residual stress intensity factor can be obtained when the residual stress filed is loaded in the elastic finite element model.

Figure 2a depicts the FE mesh for the CT specimen, and the local fine mesh distribution around the crack tip is shown in Fig. 2b. The smallest element size is $15\,\mu\mathrm{m}$, which is approximately one third of the average grain size of P92 steel (which is about $40\,\mu\mathrm{m}$ to $50\,\mu\mathrm{m}$). The model in Fig. 2 contains 8802 eight-node linear grid reduced integration elements (C3D8R) and 11060 nodes. All analyses are carried out using ABAQUS code (Hibbitt *et al.*, 2014).

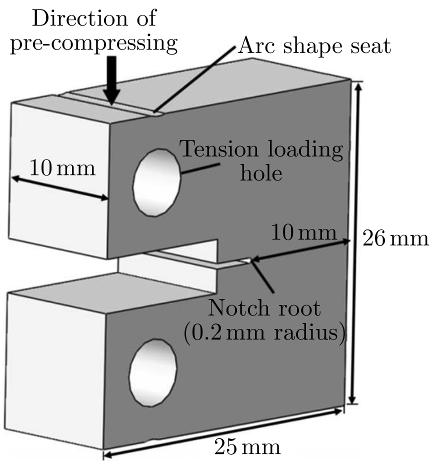

Fig. 1. Geometry of the notched compact tension (CT) specimen

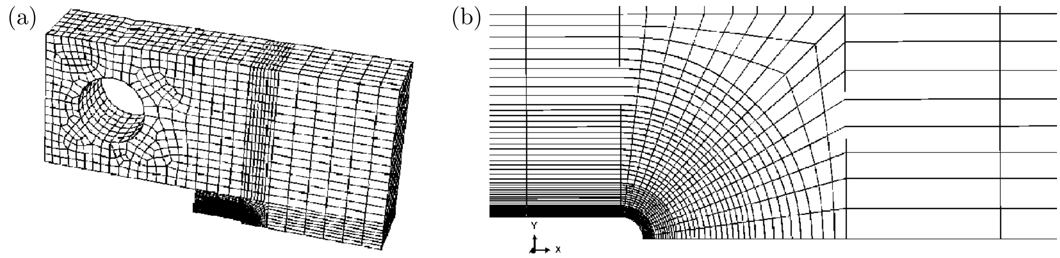

Fig. 2. Finite element model of the notched CT specimen: (a) meshes in the whole model, (b) local fine meshes around the crack tip

Different thicknesses of CT specimen, i.e. 10, 15, 25 and 30 mm, and different crack depth ratios a_0/W (a_0 and W are the initial crack depth and width, respectively) are employed. The specific geometric parameters of CT specimens are listed in Table 1.

Table 1. Geometric parameters of CT specimens used in the FEM

Specimen thickness B [mm]	Crack depth a_0/W	Pre-compressed load P [N]
10 15 20 25 30	0.3	200-20000
10 15 20 25 30	0.4	200-20000
10 15 20 25 30	0.5	200-20000
10 15 20 25 30	0.6	200-20000
10 15 20 25 30	0.7	200-20000

2.2. Material properties

The isotropic hardening model and mechanical properties of P92 steel are used. The power-hardening stress-strain relation (Song *et al.*, 2015a) at room temperature is expressed as follows

$$\sigma = \begin{cases} E\varepsilon & \sigma \leqslant \sigma_0 \\ K_P\varepsilon^{n_p} & \sigma > \sigma_0 \end{cases} \tag{2.1}$$

where E is Young's modulus of 206000 MPa. n_p is strain-hardening exponent of 0.155, σ_0 is the yeilding stress of 320 MPa, and K_p is the strain-hardening coefficient of 861 MPa (Zhao *et al.*, 2012).

3. FEM results and a method of average stress intensity factor predictions

Webster *et al.* (2011) and Zhao *et al.* (2013) obtained an average stress intensity factor K_{ave} of the residual stress by estimating average residual stress distributions. The average stress intensity factor K_{ave} is calculated by

$$K_{ave} = \sigma_{ave}\sqrt{2\pi r_{ave}} \tag{3.1}$$

where σ_{ave} is the average residual stress ahead of the crack tip, r_{ave} the average distance of residual stress distributions ahead of the crack tip.

Figure 3 shows the residual stress distribution ahead of the crack tip of the CT specimen with thickness $B = 10\,\mathrm{mm}$, crack length $a_0/W = 0.3$, and pre-compression load $P = 5000\,\mathrm{N}$. The residual stress σ_{22} is normalised by σ_0, and we could obtain the average residual stress intensity factor $K_{ave} = 224.22\,\mathrm{MPa{\cdot}mm^{-1/2}}$. Similarly, we could calculate K_{ave} values under different load levels and specimen sizes.

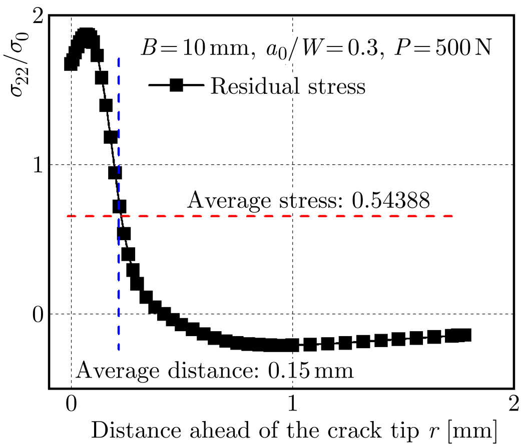

Fig. 3. The distribution of residual stress and average stress ahead of the crack tip

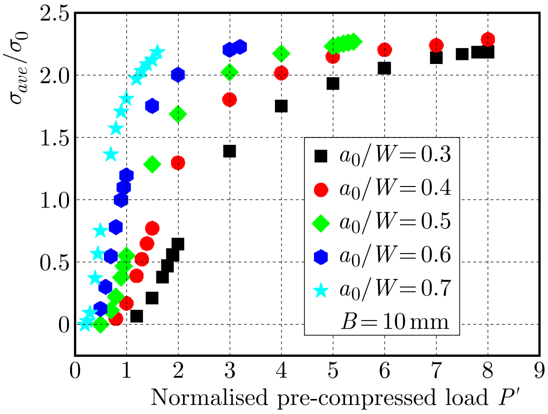

Fig. 4. Comparision of the average stress distribution under different crack depth a_0/W, specimen thickness $B = 10\,\mathrm{mm}$

Figure 4 depicts distribution of the average residual stresses σ_{ave}/σ_0 of the CT specimen with thickness $B = 10\,\mathrm{mm}$ and different crack length under different pre-compression loads. The pre-compression load P is normalised as $P' = P\,\mathrm{N}$. It is clearly seen that as the crack length a_0/W increases, the average residual stresses σ_{ave}/σ_0 grows under the same pre-compression load. In addition, σ_{ave}/σ_0 increases rapidly at a low range of the pre-compression load but tends to a constant in a high range of the load.

Figure 5 compares the simulated stress intensity factors K_{FEM} (which are directly obtained by using the history output variables from FE results) and the average residual stress intensity factors K_{ave} of the CT specimen with thickness $B = 10$ mm and different crack length under the different pre-compression loads. The distribution of K_{ave} and σ_{ave}/σ_0 with the same crack length under different pre-compression loads have the same tendency. Additionally, the distribution of K_{ave} and K_{FEM} for different pre-compression loads are also similar. It is indicated that the average stress intensity factor K_{ave} of the residual stress estimated by the average residual stress could underestimate the residual stress intensity factor, but it is much too conservative and not accurate, which may endanger in-service components. Moreover, the prediction method of the residual stress intensity factor is complex and it needs analysis of simulation. Therefore, a simple and accurate method is needed to predict the residual stress intensity factor.

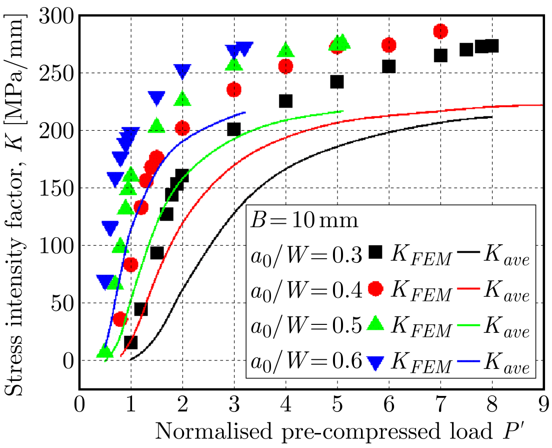

Fig. 5. Comparision of stress intensity factors between the FEM solutions and the results calculated by the average stresses

4. Methodology

The results of the normalised SIF under different specimen thickness B and different crack depth a_0/W are listed in Fig. 6. To simplify the analysis, the parameters are normalised as follows: $K' = K$ [MPa·m$^{-1/2}$], and $B' = B$ [mm]. It is found from Fig. 6 that K' increases rapidly in the low range of P' and smoothly increases in the high range of P'. The change rules of the K'-P' line may be related to the change rules of the residual stress, because the SIF is a vital term in the stress distribution near the crack tip (Tada, 2000). Moreover, for the same specimen, thickness B, K' line moves left and upward as the crack depth a_0/W increases. In addition, for the same crack depth a_0/W, the K'-P' line moves right and downward as the specimen thickness B increases.

By comparing several types of function expressions, a perfect relationship between K' and P' is approximated to a complex exponential function (Fig. 6), which can be expressed by the following equation

$$K' = ae^{bP'} + ce^{dP'} \tag{4.1}$$

K' is the normalised SIF ($K' = K$ [MPa·m$^{-1/2}$]) and P' is the normalised pre-compressed load ($P' = P$ [N]). Additionally, a, b, c and d are parameters related to the normalised specimen thickness B' ($B' = B$ [mm]) and crack depth a_0/W. All parameters for different geometrical conditions are obtained by fitting the curves, as seen in Fig. 6.

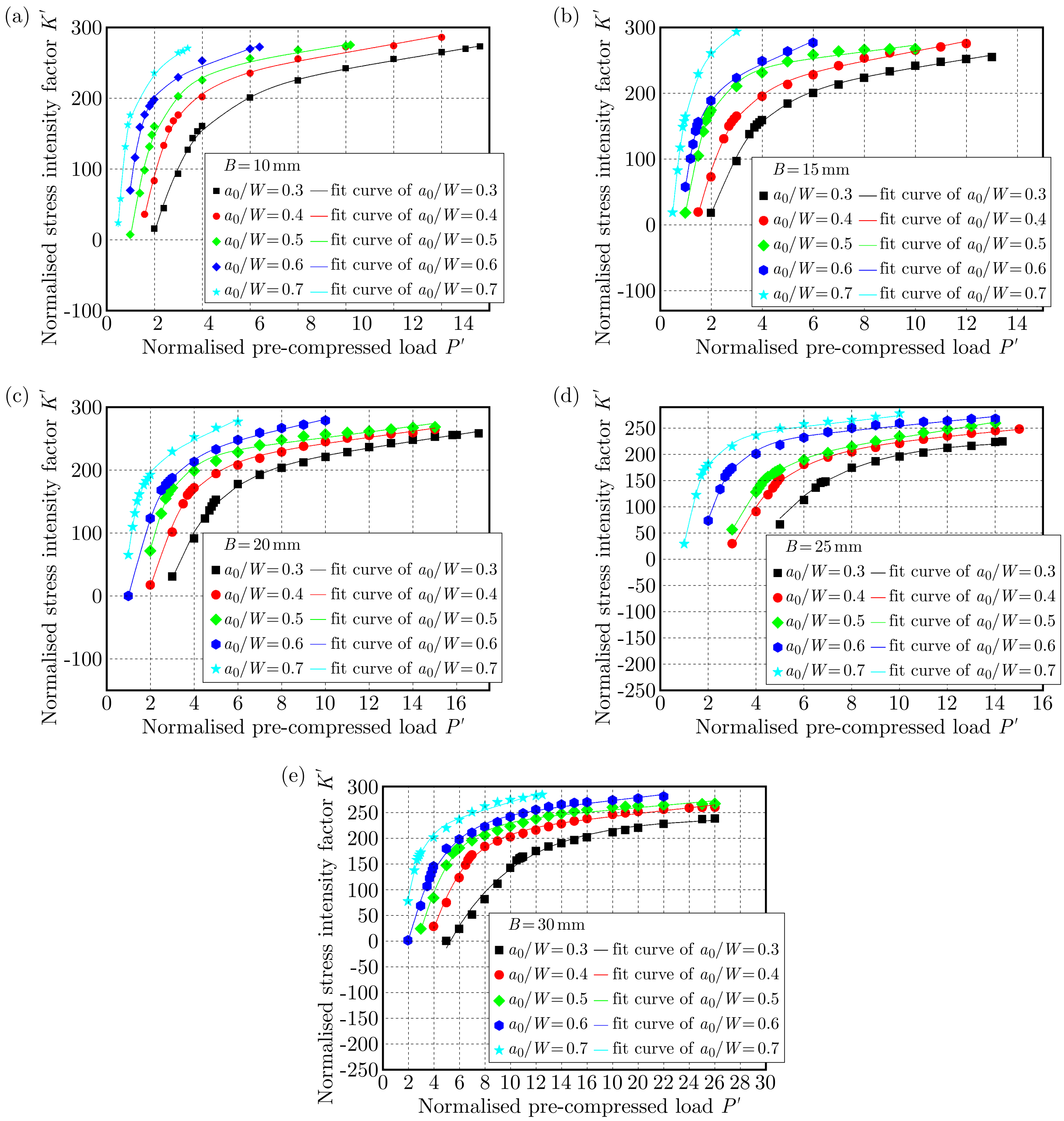

Fig. 6. Comparision of K' solutions under different crack depth a_0/W, (a) specimen thickness $B = 10$ mm, (b) $B = 15$ mm, (c) $B = 20$ mm, (d) $B = 25$ mm, (e) $B = 30$ mm

Figure 7 shows the fitted curves of parameters (a, b, c and d) and the normalised specimen thickness B' under different crack depths a_0/W. It is obvious that a-B' and c-B' curves are linear, whereas b-B' and d-B' curves are approximately quadratic. The fitted curves can be expressed as follows

$$
\begin{aligned}
a &= a_1 + a_2 B' \qquad & b &= b_1 + b_2 B + b_3 {B'}^2 \\
c &= c_1 + c_2 B' \qquad & d &= d_1 + d_2 B + d_3 {B'}^2
\end{aligned} \tag{4.2}
$$

It is indicated that as the crack depth increases, a-B' and b-B' curves move upward but c-B' and d-B' curves move downward. The variation trend in the fitted curves is constantly related to the crack depth a_0/W. Therefore, it is important to analyse the relationship between the parameters a_1, a_2, b_1, b_2, b_3, c_1, c_2, d_1, d_2 and d_3 and a_0/W.

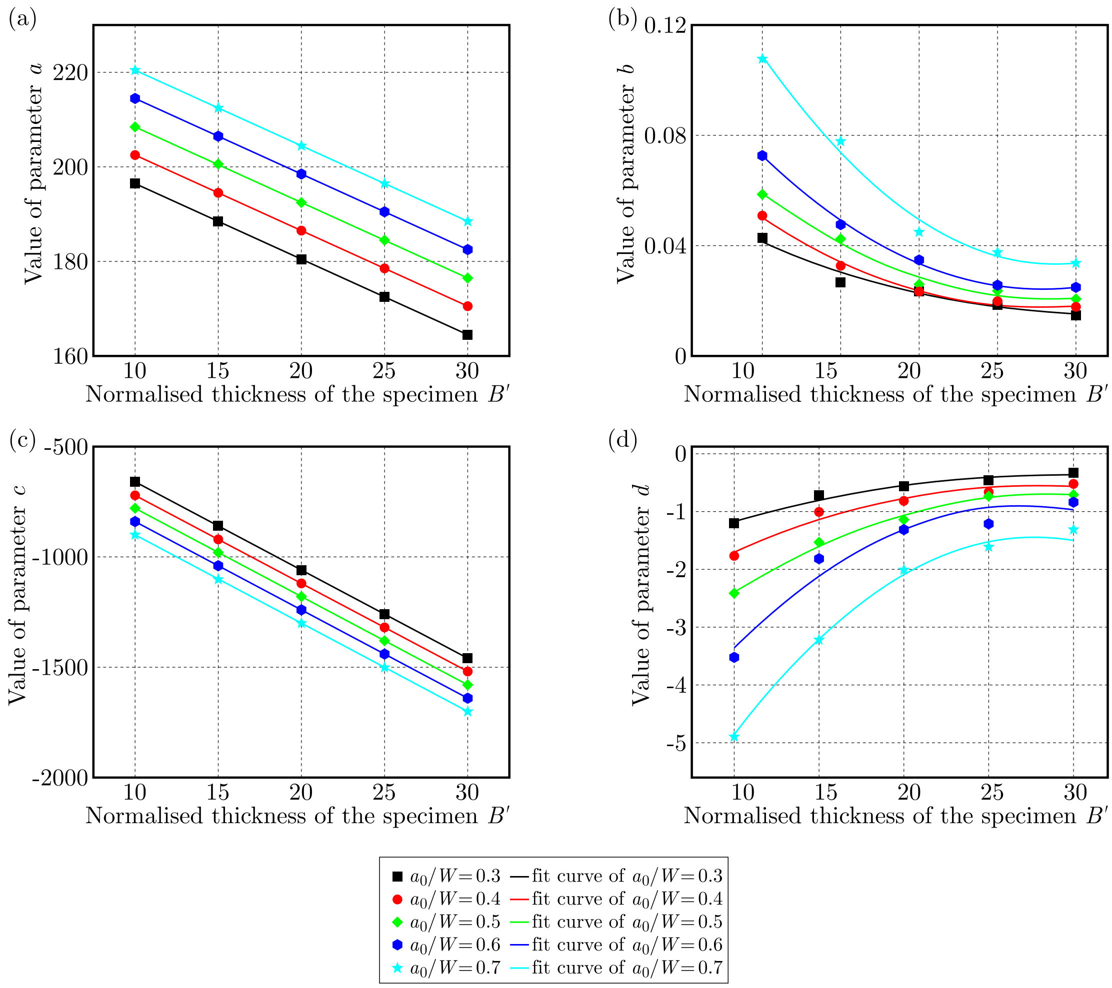

Fig. 7. Fitted curve of parameters and normalised specimen thickness B', (a) parameters a and B', (b) b and B', (c) c and B', (d) d and B'

Figure 8 shows the fitted curve of parameters a_1, a_2, b_1, b_2, b_3, c_1, c_2, d_1, d_2, d_3 and the crack depth a_0/W. It can be concluded that a_1-B' and c_1-B' curves show a good linear relationship, a_2-B' and c_2-B' curves are horizontal, and the other curves are approximately quadratic. The fitted curves can be expressed as follows

$$
\begin{array}{lll}
a_1 = a_{11} + a_{12}\dfrac{a_0}{W} & a_2 = -1.6 & b_1 = b_{11} + b_{12}\dfrac{a_0}{W} + b_{13}\dfrac{a_0}{W}^2 \\
b_2 = b_{21} + b_{22}\dfrac{a_0}{W} + b_{23}\dfrac{a_0}{W}^2 & b_3 = b_{31} + b_{32}\dfrac{a_0}{W} + b_{33}\dfrac{a_0}{W}^2 & \\
c_1 = c_{11} + c_{12}\dfrac{a_0}{W} & c_2 = -40 & d_1 = d_{11} + d_{12}\dfrac{a_0}{W} + d_{13}\dfrac{a_0}{W}^2 \\
d_2 = d_{21} + d_{22}\dfrac{a_0}{W} + d_{23}\dfrac{a_0}{W}^2 & d_3 = d_{31} + d_{32}\dfrac{a_0}{W} + d_{33}\dfrac{a_0}{W}^2 &
\end{array}
\tag{4.3}
$$

All the coefficients a_1, a_2, b_1, b_2, b_3, c_1, c_2, d_1, d_2 and d_3 obtained by fitting the curves shown in Fig. 8 are listed in Table 2.

By substituting the coefficients into Eqs. (4.3) and substituting these equations into Eqs. (4.2), we could obtain a general equation to predict the SIF of the CT specimen under the

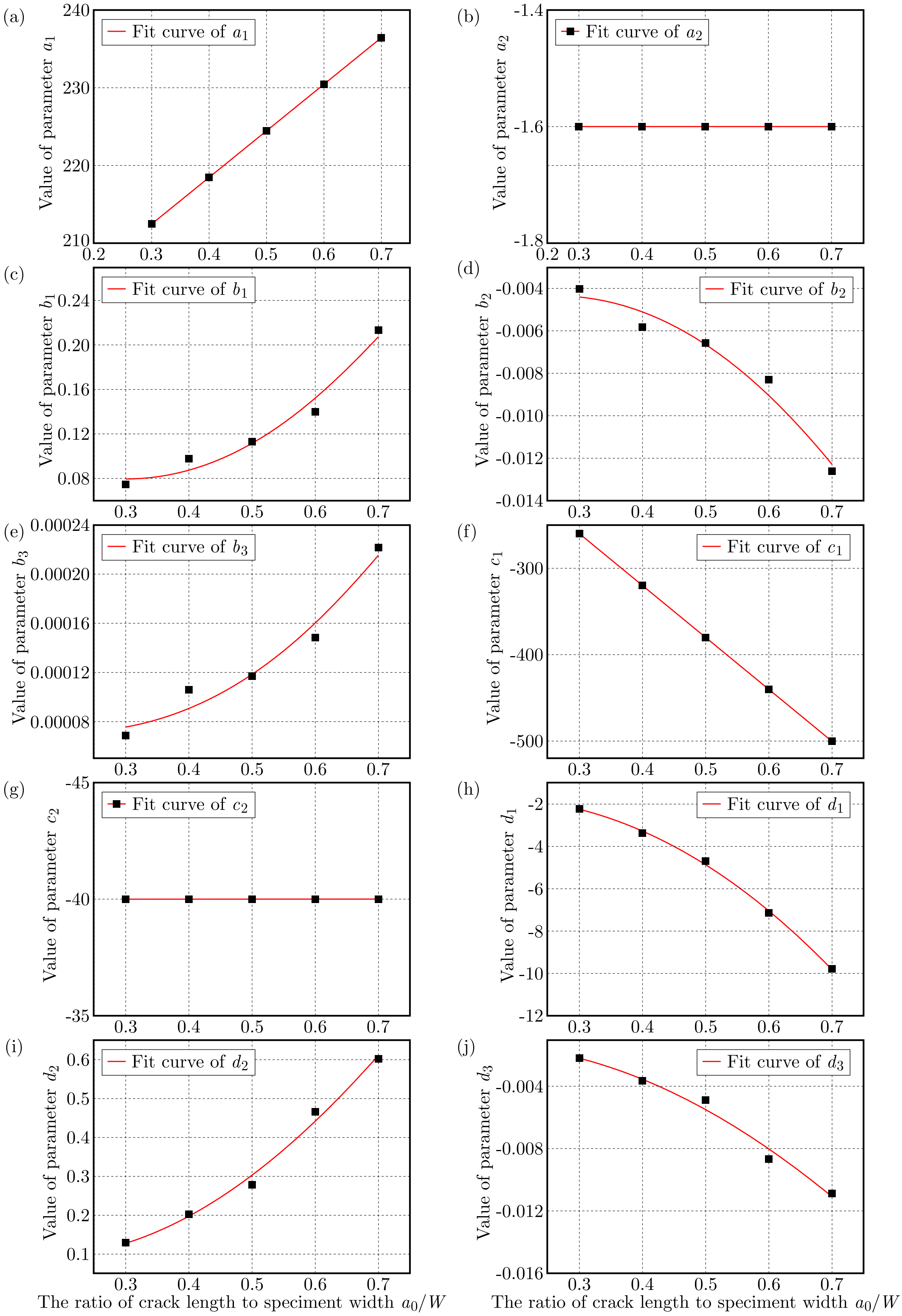

Fig. 8. Fitted curve of coefficients and normalised crack depth a_0/W: (a) a_1, (b) a_2, (c) b_1, (d) b_2, (e) b_3, (f) c_1, (g) c_2, (h) d_1, (i) d_2, (j) d_3

Table 2. Coefficients of the fitted curves in Fig. 8

a_{11}	a_{12}	a_2	b_{11}	b_{12}	b_{13}
194.5	60	−1.6	0.15075	−0.47518	0.79486
b_{21}	b_{22}	b_{23}	b_{31}	b_{32}	b_{33}
−0.0075	0.02322	−0.0429	0.00011	−0.00031	0.00066
c_{11}	c_{12}	c_2	d_{11}	d_{12}	d_{13}
−80	−600	−40	−2.831	10.815	−29.73
d_{21}	d_{22}	d_{23}	d_{31}	d_{32}	d_{33}
0.11576	−0.467	1.67914	−0.0015	0.00658	−0.0289

pre-compressed condition wherein only the following two variables are involved: specimen thickness B and crack depth a_0/W. The rearranged functions can be expressed as follows

$$
\begin{aligned}
K' = {} & \Big(a_{11} + a_{12}\frac{a_0}{W} + a_2 B'\Big)\exp\Big\{\Big[b_{11} + b_{12}\frac{a_0}{W} + b_{13}\Big(\frac{a_0}{W}\Big)^2 \\
& + \Big(b_{21} + b_{22}\frac{a_0}{W} + b_{23}\Big(\frac{a_0}{W}\Big)^2\Big)B + \Big(b_{31} + b_{32}\frac{a_0}{W} + b_{33}\Big(\frac{a_0}{W}\Big)^2\Big)B'^2\Big]P'\Big\} \\
& + \Big(c_{11} + c_{12}\frac{a_0}{W} + c_2 B'\Big)\exp\Big\{\Big[d_{11} + d_{12}\frac{a_0}{W} + d_{13}\Big(\frac{a_0}{W}\Big)^2 \\
& + \Big(d_{21} + d_{22}\frac{a_0}{W} + d_{23}\Big(\frac{a_0}{W}\Big)^2\Big)B + \Big(d_{31} + d_{32}\frac{a_0}{W} + d_{33}\Big(\frac{a_0}{W}\Big)^2\Big)B'^2\Big]P'\Big\}
\end{aligned}
\tag{4.4}
$$

5. Verification of the function

To validate the function, we compare the SIFs between the FE method results, the calculated solutions obtained by this function and the average residual stress intensity factors. The follwing two cases of CT specimens with different geometry are chosen for the study under the pre--compressed condition:

- Case 1: specimen thickness $B = 18\,\mathrm{mm}$ and the crack depth $a_0/W = 0.35$;
- Case 2: specimen thickness $B = 28\,\mathrm{mm}$ and the crack depth $a_0/W = 0.65$.

First, according to Eq. (4.4), we can obtain specific calculation equations for specimens of each geometry under the pre-compressed condition. After substituting different normalised pre--compressed loads P' into the equations, the data of the normalised SIF K' can be obtained.

It can be seen from Fig. 9 that the calculated solutions are a good fit to the FE solutions, and the function is more appropriate and larger than the average residual stress intensity factors. In conclusion, this approach is satisfactory and accurate in enabling the engineering estimates for fracture related problems.

6. Conclusions

The finite-element method is applied to assess the effects of local tensile residual stress on the stress intensity factor. A simple method for calculating Mode I stress intensity factor of residual stress is presented. The main results obtained are summarized as follows:

- As the crack length a_0/W increases, the average residual stresses σ_{ave}/σ_0 grows, under the same pre-compression load. σ_{ave}/σ_0 increases rapidly at the low range of the pre--compression load but tends to a constant value in the high range of load.

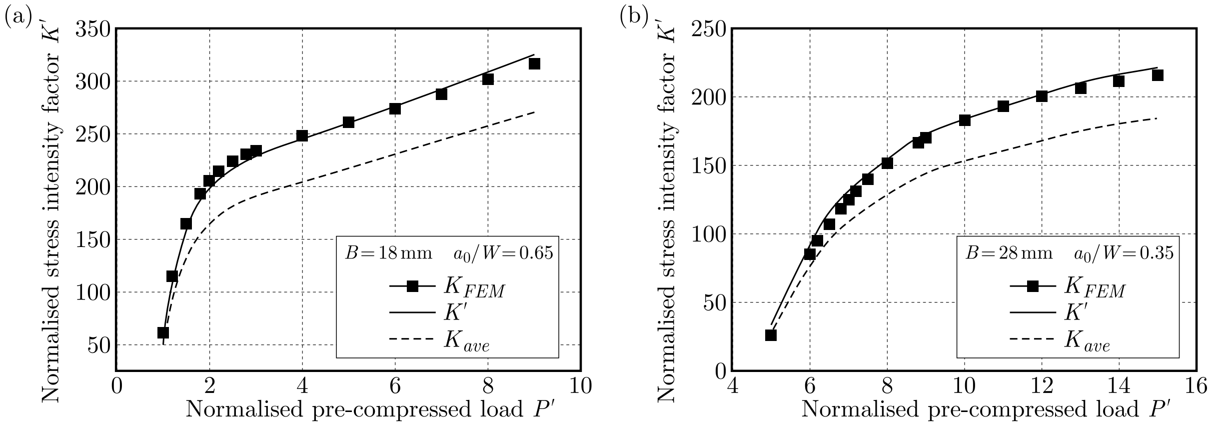

Fig. 9. Comparison of K' between the FE solutions, average results and calculated solutions: (a) specimen thickness $B = 18$ mm, crack depth $a_0/W = 0.35$, (b) $B = 28$ mm, $a_0/W = 0.65$

- The distributions of average residual stress intensity factors K_{ave} and σ_{ave}/σ_0 of the CT specimen with the same crack length under different pre-compression loads have the same tendency. Additionally, the distribution of K_{ave} and K_{FEM} under different pre-compression loads are also similar. Nevertheless, K_{ave} estimated by the average residual stress is too conservative and not accurate. The method is complex and needs analysis of simulation results.
- A simple method for calculating Mode I stress intensities for the CT specimen under the pre-compressed condition is proposed. The approach is very easy and simple, which consists of two variables only if the geometry is defined: specimen thickness B and the crack depth a_0/W. A comparison between the calculation and FE solutions suggests that the approach is satisfactory and accurate in estimating Mode I stress intensities for the CT specimen under the pre-compressed condition for engineering fracture related problems.

Acknowledgements

The author would like to acknowledge the support from the Fundamental Research Funds for the Central Universities (grant No. 3122021083).

References

1. Anderson T.L., 2005, *Fracture Mechanics: Fundamentals and Applications*, CRC Press
2. ASTM, 2013, Standard Test Method for Measurement of Creep Crack Growth Times and Rates in Metals, 27
3. Bower A.F., 2009, *Applied Mechanics of Solids*, CRC Press
4. Chen L.Y., Wang G.Z., Tan J.P., Xuan F.Z., Tu S.T., 2013a, Effects of residual stress on creep damage and crack initiation in notched CT specimens of a Cr-Mo-V steel, *Engineering Fracture Mechanics*, **97**, 80-91
5. Erdogan F., 1962, On the stress distribution in plates with collinear cuts under arbitrary loads, *Proceedings of the Fourth US National Congress of Applied Mechanics*, **1**, 547-574
6. Hibbitt, Karlsson & Sorensen, Inc, 2014, ABAQUS version 6.14
7. Isida M., 1966, Stress intensity factors for the tension of an eccentrically cracked strip, *ASME, Journal of Applied Mechanics*, **33**, 3, 674-675
8. Nikbin K.M., 2004, Justification for meso-scale modeling in quantifying constraint during creep crack growth, *Materials Science and Engineering: A*, **365**, 107-113

9. O'Dowd N.P., Nikbin K.M., Biglari F.R., 2005, Creep crack initiation in a weld steel: effects of residual stress, *Proceedings of 2005 ASME Pressure Vessels and Piping Division Conference*, Denver, Colorado, USA, 843-851
10. Rooke D.P., Percy D.J., 1976, *Compendium of Stress Intensity Factors*, HMSO Ministry of Defence, Procurement Executive
11. Shirahatti A.M., Hossain S., Smith D.J., 2014, The effect of combined applied and residual stress on creep crack initiation in stainless steel, *Procedia Engineering*, **86**, 669-676
12. Sih G.C., Macdonald B., 1974, Fracture mechanics applied to engineering problems-strain energy density fracture criterion, *Engineering Fracture Mechanics*, **6**, 2, 361-386
13. Sih G.C., Paris P.C., Erdogan F., 1974, Crack-tip stress intensity factors for the plane extension and plate bending problems, *Journal of Applied Mechanics*, **29**, 306-312
14. Sneddon I.N., 1946, The distribution of stress in the neighbourhood of a crack in an elastic solid, *Proceedings of the Royal Society A*, **187**, 1009, 229-260
15. Song X.M., Wang G.Z., Tu S.-T., Xuan F.Z., 2015a, Effects of residual stress on creep crack initiation and growth of Cr-Mo-V steel in cracked C(T) specimen, *Procedia Engineering*, **130**, 1770-1778
16. Song X.M., Wang G.Z., Xuan F.Z., Tu S.T., 2015b, Investigation of residual stress effects on creep crack initiation and growth using local out-of-plane compression, *Engineering Fracture Mechanics*, **149**, 45-57
17. Tada H., Paris P.C., Irwin G.R., 2000, *The Stress Analysis of Cracks Handbook*, American Society of Mechanical Engineers
18. Turski M., Bouchard P.J., Steuwer A., Withers P.J., 2008, Residual stress driven creep cracking in AISI Type 316 stainless steel, *Acta Materialia*, **56**, 3598-3612
19. Webster G.A., Davies C.M., Nikbin K.M., 2011, Prediction of creep crack growth in the presence of residual stress, *Materials at High Tempertures*, **28**, 3, 165-171
20. Xu M., Chen J., Lu H., Xu J., Yu C., Wei X., 2016, Effects of residual stress and grain boundary character on creep cracking in 2.25Cr-1.6W steel, *Materials Science and Engineering: A*, **659**, 188-197
21. Zhao L., Jing H., Xu L., An J., Xiao G., 2012, Numerical investigation of factors affecting creep damage accumulation in ASME P92 steel welded joint, *Materials Design*, **34**, 566-575
22. Zhao L., Jing H., Xu L., Han Y., Xiu J., 2013, Effect of residual stress on creep crack growth behavior in ASME P92 steel, *Engineering Fracture Mechanics*, **110**, 233-248

Manuscript received September 20, 2022; accepted for print October 10, 2022